Macromolecules

Article

pubs.acs.org/Macromolecules

Interactive Crystallization Kinetics in Double-Crystalline Block Copolymer

Ming-Champ Lin,[†] Hsin-Lung Chen,*[,†] Wen-Bin Su,[‡] Chun-Jen Su,[‡] U-Ser Jeng,[‡] Fu-Yuan Tzeng,[§] Jheng-Yuan Wu,[§] Jing-Cherng Tsai,[§] and Takeji Hashimoto[†,⊥]

[†]Department of Chemical Engineering and Frontier Center of Fundamental and Applied Sciences of Matters, National Tsing Hua University, Hsin-Chu 30013, Taiwan

[‡]National Synchrotron Radiation Research Center, Hsin-Chu 300, Taiwan

[§]Department of Chemical Engineering, National Chung Cheng University, Chia-Yi 62142, Taiwan

[⊥]Advanced Science Research Center, Japan Atomic Energy Agency, Naka-gun, Ibaraki Pref. 319-1195, Japan

Supporting Information

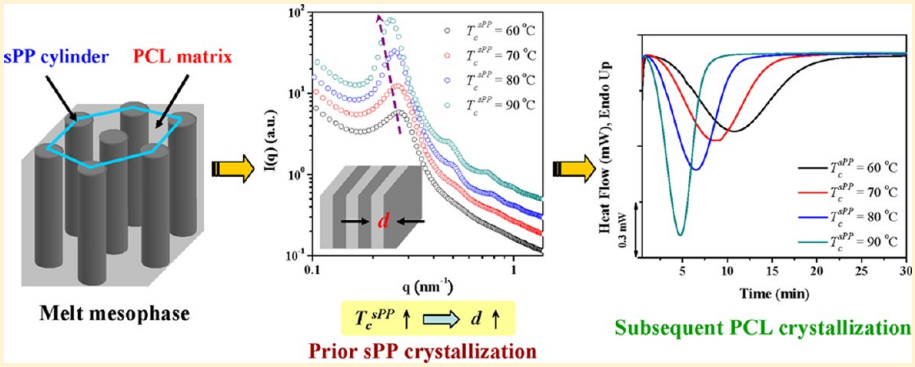

ABSTRACT: The crystallization kinetics and crystallization-induced morphological formation of an asymmetric double-crystalline block copolymer, syndiotactic polypropylene-*block*-poly(ε-caprolactone) (sPP-*b*-PCL), have been investigated by time-resolved simultaneous small-angle and wide-angle X-ray scattering (SAXS/WAXS). The sPP-*b*-PCL under study exhibited hexagonally packed cylinder morphology in the melt state, where the minority sPP block formed the cylindrical microdomains dispersed in the PCL matrix. The crystallization behavior was studied by imposing two types of crystallization histories: (1) two-stage crystallization, where the diblock was first cooled to the temperature T_c^{sPP} situating between the melting points of the two components ($T_m^{PCL} < T_c^{sPP} < T_m^{sPP}$) to allow sPP crystallization to saturation followed by cooling to $T_c^{PCL} < T_m^{PCL}$ to induce PCL crystallization; (2) one-stage crystallization, where the system was cooled directly to $T_c < T_m^{PCL}$ to allow the two components to crystallize competitively. In both cases, the crystallization of sPP block was in general able to disrupt the melt structure and transformed it into a crystalline lamellar morphology. For the two-stage crystallization process, the PCL block was found to exhibit a faster crystallization at a given T_c^{PCL} when the sPP block was precrystallized at higher T_c^{sPP}. This "interactive crystallization kinetics" was attributed to the mediation of the stretching of PCL blocks by the thickness of sPP crystalline domains which depended on T_c^{sPP}. In the one-stage process, the crystallization events of the two blocks became more competitive with decreasing T_c. The morphological perturbation induced by crystallization was also more hindered at lower T_c, such that a significant portion of sPP blocks remained confined within the cylindrical microdomains so as to suppress the sPP crystallinity.

INTRODUCTION

Self-assembly of diblock copolymer can generate a variety of long-range ordered microdomains, such as lamellae, bicontinuous gyoid, hexagonally packed cylinders, and BCC-packed spheres, depending on the segregation strength and the volume fraction of the constituting blocks.[1−5] The resultant nanoscale microdomains can be employed as templates for providing long-range ordered spatial confinement with well-defined geometries. Incorporation of crystallizable blocks into block copolymers thus offers an effective way to explore polymer crystallization behavior under nanoscale confinement.

The crystallization behavior and the structure formation of diblock copolymers composing of one crystalline block (C) and one amorphous block (A) (i.e., the C−A diblocks) have been subjected to extensive studies.[6−23] It has been established that

Received: April 6, 2012
Revised: May 26, 2012
Published: June 8, 2012

the interblock segregation strength, the order−disorder transition temperature (T_{ODT}), the glass transition temperature of A block (T_g^A), and the crystallization driving force of C block (governed by the crystallization temperature, T_c) are the major factors that control the extent of confinement to the crystallization process. At $T_c < T_g^A < T_{ODT}$, the confinement on the crystallization of C block is strong since the crystallization is restricted within the C microdomains surrounded by the hard glassy matrix formed by A block.[6−11] Such a confinement effect is called "hard confinement". In the case where $T_g^A < T_c < T_{ODT}$ (where the amorphous phase remains soft upon crystallization), the crystallization of C block may still be effectively confined once the segregation strength of two blocks is high, and the amorphous matrix is said to impose a "soft confinement" to the crystallization.[12−18] Both the hard and soft confinements have drastic impacts on the overall crystallization kinetics.[12−15] On the other hand, when the crystallization of C block takes place in the weakly segregated system, the crystallization process may break out of the initial microdomains to form crystalline extended lamellar domains.[19−23]

Most research of crystalline diblock copolymers has focused on the C−A diblocks, while the systems containing two crystalline blocks (i.e., the double-crystalline dibocks or C−C diblocks) have started to be attracted attention over the past decade. The crystallization behavior and the nanostructure formation of this type of system are expected to be much more complex because of the additional competition between the crystallization events of the two crystalline components.[24,25] If the two blocks (C_1 and C_2) exhibit largely different melting points (T_m^{c1} and T_m^{c2} with $T_m^{c1} > T_m^{c2}$), a two-stage crystallization history may be implemented, where the diblock is first cooled to $T_m^{c2} < T_c < T_m^{c1}$ to induce crystallization of C_1 block followed by cooling to $T_c < T_m^{c2}$ to allow C_2 block to crystallize.[26−34] The crystallization of the first-crystallized C_1 component may destroy the preexisting microphase-separated structure in the same way as weakly segregated crystalline−amorphous block copolymers. If the segregation strength is sufficiently high, the crystallization of the leading block will not disrupt the melt mesophase. In both cases, the C_2 component which crystallizes subsequently may be left within the confined space established by the crystallization of C_1 block.

When the diblock is rapidly cooled from the melt state to T_c situating below both T_m^{c1} and T_m^{c2} (i.e., the one-stage crystallization), a competitive and/or concurrent crystallization between the two components may take place. Such a competition in crystallization coupled with its interplay with the segregation power of the microphase-separated domains should be the key that determines the crystalline morphology.[35−43]

The detailed mechanism and the underlying principles governing the structural formation of double-crystalline block copolymers remain largely unresolved. Most previous studies have reported the change in morphology upon crystallization (induced by either stepwise cooling or crystallization at a given temperature) based on the ultimate morphology observed after the completion of crystallization.[28,29,33,34,38,41] The transient morphological transformation of C−C diblocks during isothermal crystallization has indeed not been investigated in detail. To comprehensively resolve this issue, the simultaneous small-angle X-ray scattering/wide-angle X-ray scattering (SAXS/WAXS) technique with the synchrotron radiation source was employed here to promptly collect the data during the crystallization process. Here, the SAXS/WAXS measurements were conducted with a temperature-jump cooling system, which allowed very rapid cooling and thermal equilibration at the prescribed T_c within a few seconds. In addition to the two-stage crystallization history that has been frequently implemented for the C−C diblocks,[29−31] we further concentrated on the competitiveness of the two crystallization events in the one-stage crystallization process, which has been rarely studied for the systems with the two crystalline blocks exhibiting largely different melting points.

In this study, we mainly investigate the kinetics of the crystallization as well as the nanostructure formation of a double-crystalline block copolymer. The simultaneous SAXS/WAXS experiments allow both the structural formation and the crystallinity development during the crystallization under different conditions to be monitored concomitantly. In particular, the interplay between the crystallization processes of the two crystalline blocks will be revealed from this study.

The block copolymer system investigated here is an asymmetric syndiotactic polypropylene-*block*-poly(ε-caprolactone) (sPP-*b*-PCL) with the volume fraction of sPP block of 0.24. sPP and PCL are both crystalline polymers with the nominal melting points of ca. 110 and 55 °C, respectively,[44] as represented by the peak temperatures of the melting endotherms. The relatively large disparity in melting points between these two components allows the system to crystallize over a broad range of conditions for tuning the competitiveness and interplay of the two crystallization events. On basis of this fact, it will be shown that the crystallization kinetics of PCL block was dramatically affected by the crystallization temperature of the prior sPP crystallization. Recently, Cong et al. reported similar interactive crystallization behavior in a weakly segregated symmetric C−C diblock of poly(L-lactide)-*block*-poly(ethylene oxide) (PLLA-*b*-PEO).[34] Because microphase separation was inaccessible for this system, the crystallization of the leading crystalline PLLA block occurred from the disordered state. This crystallization event then dominated the morphological formation so as to prescribe the confinement environment and the degree of stretching for the PEO block, which in turn influenced the kinetics of PEO crystallization below T_m^{PEO}. The interactive crystallization kinetics observed in the present sPP-*b*-PCL was distinguished from that of PLLA-*b*-PEO in the sense that the crystallization of the leading crystalline sPP component occurred from the microphase-separated melt, such that the crystallization-induced morphological perturbation was governed by the balance between the crystallization driving force of sPP and the segregation strength that tends to stabilize the melt mesophase. Moreover, the composition of the sPP-*b*-PCL under study was highly asymmetric with the minority sPP blocks forming cylindrical microdomains dispersed in the continuous PCL matrix; it is interesting to show that even the crystallization of the minority sPP block (which led to a moderate level of crystallinity) could still influence the stretching of the majority PCL block and thus affect its crystallization kinetics. These results may provide significant insights into the strategy for controlling the crystallization-induced nanostructure formation of double-crystalline block copolymers.

■ EXPERIMENTAL SECTION

Materials. The detailed synthetic method for preparations of sPP-*b*-PCL was described in the previous report.[44] In brief, the diblock copolymer was synthesized by controlled ring-opening polymerization

dx.doi.org/10.1021/ma300711k | Macromolecules 2012, 45, 5114−5127

of ε-caprolactone using aluminum alkoxide-terminated sPP as the macroinitiator. The aluminum alkoxide-terminated sPP macroinitiator (M_n = 2430, M_w/M_n = 1.49, sydiotacticity (*rrrr*) = 74.45%) was generated by activation of the OH-capped sPP with trialkyaluminum, whereas the OH-capped sPP was synthesized by the selective chain transfer reaction to triethylaluminum during syndiospecific polymerization of propylene in the presence of syndiospecific metallocene catalyst.

The molecular weights of sPP and PCL blocks were 2430 and 9870 g/mol, respectively, as determined by high-temperature GPC (in 1,2,4-trichlorobenzene at 135 °C); hence, the volume fraction of the constituting sPP block was 0.24 prescribed by the corresponding molecular weights and the relevant densities of sPP and PCL blocks in the melt state. The polydispersity index of this copolymer was found to be 1.14; such a low polydispersity resulted in microphase separation to form highly ordered microdomains. Detailed molecular characteristics and the thermal properties of this diblock copolymer have been described elsewhere.[44]

Bulk Sample Preparation. The bulk samples of sPP-*b*-PCL were prepared by dissolving the diblock copolymer in tetrahydrofuran (THF) at 70 °C. The concentration of the polymers in the solution was 5 wt %. The samples were subsequently cast onto the Petri dish followed by a slow evaporation of the solvent at 30 °C for 2 days. The samples were further dried in vacuum at 60 °C for 2 h and then at room temperature for 4 days for complete solvent removal.

Differential Scanning Calorimetry (DSC) Measurement. DSC experiments were carried out by a Perkin-Elmer DSC-7 instrument to study the isothermal crystallization and melting behavior of the diblock copolymer. Samples of ca. 5 mg were encapsulated in aluminum pans. The calibration was performed with indium and hexatricontan, and all tests were run using ultrapure nitrogen as purge gas.

The isothermal crystallization experiments were carried out for both sPP and PCL blocks within sPP-*b*-PCL. In order to investigate the crystallization kinetics of sPP block, the sample was first heated to 170 °C (which is at least 40 °C higher than the nominal melting points of sPP and PCL blocks (i.e., T_m^{sPP} and T_m^{PCL}) but lower than T_{ODT} of sPP-*b*-PCL) and kept at this temperature for 10 min to erase the previous thermal history. The sample was then cooled (at 80 °C/min) to the prescribed isothermal crystallization temperature T_c^{sPP} (at $T_m^{PCL} < T_c^{sPP} < T_m^{sPP}$), and the crystallization process of sPP was monitored as a function of time.

To evaluate the effect of the crystallization temperature of sPP block on the kinetics of the subsequent crystallization of PCL block, the sample was heated to 170 °C and annealed at this temperature for 10 min to remove the previous thermal history, followed by prompt cooling (at 80 °C/min) to a temperature in the range of $T_m^{PCL} < T_c^{sPP} < T_m^{sPP}$ (where PCL blocks remained molten state) for isothermal crystallization of sPP. After the crystallinity of sPP block at each T_c^{sPP} reached saturation, the sample was cooled to 41.5 °C < T_m^{PCL} at which the crystallization exotherm of PCL block was recorded. All the samples after the isothermal crystallization treatments were eventually heated to 190 at 10 °C/min to record the melting endotherms of sPP and PCL crystals formed.

Time-Resolved Simultaneous SAXS/WAXS Measurements. Simultaneous SAXS/WAXS experiments were performed at Beamline 23A1 at the National Synchrotron Radiation Research Center (NSRRC) located at Hsin-Chu, Taiwan.[45] A two-dimensional Mar CCD detector with 512 × 512 pixel resolution was used to record the SAXS pattern. The energy of the X-ray source and the sample-to-detector distance were 10 keV and 2444 mm, respectively. The time necessary for each data collection was 20 s. The SAXS intensities obtained were plotted against $q = 4\pi \sin(\theta/\lambda)$, where λ is the wavelength of X-ray (λ = 0.124 nm) and 2θ is the scattering angle. The beam center was calibrated using silver behenate with the primary reflection peak at 1.076 nm^{-1}. The WAXS profiles were simultaneously collected with the SAXS profiles using a linear detector, covering the scattering vector range of 8−17.5 nm^{-1}. The WAXS angular scale was calibrated using silicon, sodalite, and high-density polyethylene.

SAXS/WAXS Data Analysis. The SAXS intensity profiles obtained from the time-resolved experiment were further used to calculate the normalized scattering invariants (Q) as a function of time during the crystallization process via

$$Q(t) = \frac{\int_0^\infty I(q; t) q^2 \, dq}{\int_0^\infty I(q; t_\infty) q^2 \, dq}$$

where the last data profile collected during crystallization at a given T_c was taken as the SAXS profile at $t \to \infty$. Since the experimentally accessible q range is finite, extrapolation to both low and high q is necessary for the integration in the above equation. In the present work, extrapolation to zero q was accomplished by applying the Debye−Bueche model,[46,47] whereas the Porod−Ruland model[48] was used for extension to large q.

Analogous to obtaining the relative invariant from SAXS profiles, the degrees of crystallinity (X_c) of sPP and PCL blocks were determined from the WAXS profiles by integrating the area under the crystalline diffraction peaks (A_c) and the amorphous halo (A_a) via

$$X_c = \frac{A_c}{A_c + A_a}$$

The deconvolution of the peaks in the WAXS profiles was performed with the PeakFit v4.11 software, assuming Gaussian function for each peak.

Polarized Optical Microscopy (POM). An Olympus BX51 microscope equipped with an Olympus DSLR E-620 digital camera and two Linkam HFS 91 hot stages (the accuracy of sample temperature control was ±0.5 °C) was used to observe the superstructure morphology during isothermal crystallization. Measurements were made in transmission under cross polarizers at 500× magnification. The specimen sandwiched between two microscope cover glasses was annealed at 170 °C on a Linkam hot stage for 10 min to erase the previous thermal history. The sample was then quickly transferred onto another Linkam hot stage pre-equilibrated at the crystallization temperature (i.e., T_c^{sPP} = 80 or 60 °C) to allow sPP crystallization. After sPP crystallized to saturation, the specimen was transferred to another hot stage pre-equilibrated at 41.5 °C to induce PCL crystallization. The development of the crystalline superstructure was then observed during PCL crystallization.

RESULTS AND DISCUSSION

1. Melt Structure and Crystallization-Induced Structure Perturbation. sPP-*b*-PCL is a double-crystalline system with both sPP and PCL blocks being crystallizable. Here we have examined the crystallization process under two types of cooling histories from the microphase-separated melt. The first type is called "two-stage crystallization", where the system was cooled from 170 °C (which is higher than T_m^{PCL} and T_m^{sPP}) to T_c^{sPP} (which is higher than $T_m^{PCL} \approx 55$ °C but lower than $T_m^{sPP} \approx 110$ °C) to allow sPP crystallization followed by cooling to T_c^{PCL} (which is lower than T_m^{PCL}) to induce PCL crystallization. The other type is called "one-stage crystallization", where the system was directly quenched from 170 °C to T_c, at which sPP and PCL blocks may compete to crystallize when T_c is sufficiently low (T_c < 41.5 °C as will be shown in subsection 3).

We first examine the melt structure of the sPP-*b*-PCL and the perturbation of melt mesophase induced by crystallization. Figure 1 shows the SAXS profiles of sPP-*b*-PCL collected at different temperatures in a two-stage cooling process. At 170 °C where both sPP and PCL blocks were in the melt state ($T_m^{PCL} < T_m^{sPP} < 170$ °C $< T_{ODT}$), the SAXS profile showed multiple scattering peaks with the position ratio of $1:3^{1/2}:4^{1/2}:7^{1/2}:9^{1/2}$. This indicated that the sPP-*b*-PCL exhibited a hexagonally packed cylinder morphology, where the minority sPP blocks formed the cylindrical microdomains dispersed in the PCL matrix. The interdomain distance (D)

dx.doi.org/10.1021/ma300711k | Macromolecules 2012, 45, 5114−5127

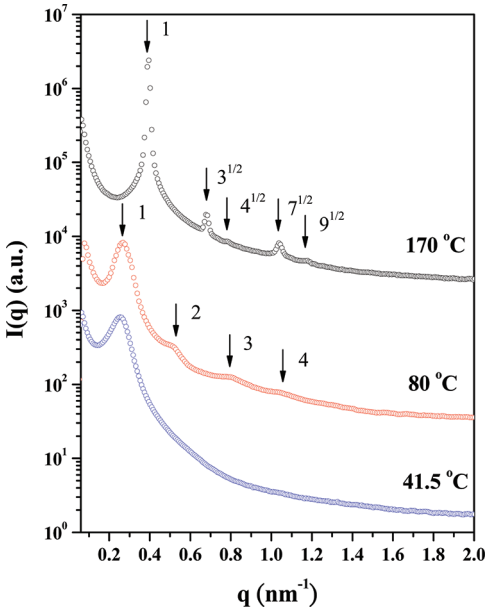

Figure 1. SAXS profiles of sPP-*b*-PCL subjecting to a two-stage cooling history. The top curve was collected at 170 °C. The middle profile was obtained by cooling the diblock from 170 to 80 °C followed by crystallization of sPP block for 20 min. The bottom profile was collected by further cooling the sample to 41.5 °C to allow PCL crystallization for 15 min.

calculated from the primary peak position was 18.5 nm and the average radius (R) of the sPP cylinder was 4.8 nm as derived from its volume fraction in the melt state (f_{sPP} = 0.24).

When the sPP-*b*-PCL was quenched to 80 °C (where T_m^{PCL} < 80 °C < T_m^{sPP} < T_{ODT}) and kept at this temperature for 20 min, sPP crystallization took place in the cylindrical microdomains surrounded by the soft PCL phase. In this case, the sPP-*b*-PCL was a crystalline−amorphous system, and the crystallization process of sPP block could perturb the melt mesophase as long as the segregation strength is not strong. The segregation strength χN (where χ is the Flory−Huggins interaction parameter and N is the degree of polymerization) at 170 °C was found to be 47.7 based on our previous calculation;[44] therefore, this diblock exhibited the intermediate segregation strength (10.5 < χN < 100).[49] It can be seen from Figure 1 that the primary peak in the SAXS profile shifted to lower q and became broader (comparing to that observed at 170 °C) upon sPP crystallization, indicating that the morphological perturbation did take place. Such a perturbation could be either a breakout of the cylindrical microdomains to form crystalline lamellar morphology or local distortion of the cylindrical microdomains. Considering that the primary peak was accompanied by three distinct higher-order peaks with integral position ratio, we concluded that the crystallization of sPP block should have disrupted the melt structure and transformed it into a crystalline lamellar morphology with the interlamellar distance of 24.2 nm. This type of breakout crystallization has been reported for crystalline−amorphous diblock copolymers with minor crystalline component.[19−23] In this case, the driving force of crystallization overwhelmed that stabilizing the melt mesophase due to relatively weak segregation strength of the copolymer, such that the crystal growth front broke out the cylindrical domains to form extended lamellar domains with a larger interdomain distance.

The breakout crystallization of sPP block can be further demonstrated by monitoring the development of crystallinity during the crystallization at 80 °C using DSC. The isothermal crystallization exotherm of sPP block in sPP-*b*-PCL crystallized at 80 °C is shown in the inset of Figure S1. The data were quantitatively analyzed by the Avrami equation:[50]

$$X_c(t) = 1 - \exp(-Kt^n)$$

where $X_c(t)$ is the relative crystallinity accumulated as of time t, the exponent n depends on the nucleation mechanism and the crystal growth geometry, and K is the overall transformation rate constant. The Avrami analysis[51] (see Figure S1 of Supporting Information) showed that the development of crystallinity followed a sigmoidal curve corresponding to the Avrami exponent of ca. 2.3. This means that the crystallization was predominantly initiated by heterogeneous nucleation followed by long-range crystal growth proceeding through breaking out the originally formed cylindrical microdomains in the melt state.[9] Moreover, our previous study revealed that the freezing (crystallization) temperature of sPP block was depressed by only 16 °C as compared to that of the corresponding sPP homopolymer during cooling from the microphase-separated melt.[44] If the crystallization of sPP block was largely confined within the cylindrical microdomain, the process should have occurred through homogeneous nucleation, which requires much larger undercooling.[12] Therefore, all the results indicated that the morphological transformation observed here should be associated with the breakout process induced by sPP crystallization.

After sPP had crystallized to saturation at 80 °C, the diblock was further quenched to 41.5 °C to induce the crystallization of PCL block (i.e., a two-stage crystallization process). This crystallization process further broadened the primary SAXS peak and diminished the higher-order peaks, indicating that PCL crystallization reduced the coherent order of the lamellar stacking.

2. Interactive Crystallization Kinetics in the Two-Stage Crystallization Process. Figures 2a and 2b show the time-resolved SAXS and WAXS profiles of the sPP-*b*-PCL, respectively, subjected to a two-stage crystallization process. Here the diblock was first quenched from 170 to 80 °C (where T_m^{PCL} < 80 °C < T_m^{sPP}) to allow sPP crystallization for 20 min, followed by quenching to 41.5 °C (41.5 °C < T_m^{PCL}) to induce PCL crystallization. At 170 °C, the SAXS profile displayed the scattering peaks associated with hexagonally packed sPP cylinder morphology in the melt state (cf. the red curve in Figure 2a). When the system was just brought to 80 °C, the SAXS peaks grew in intensity and shifted to lower q, corresponding to an increase of D by 1.85 nm (cf. the blue curve in Figure 2a). Since the swelling of D took place before the development of sPP crystallinity, it should arise from the increasing stretching of both amorphous sPP and PCL blocks normal to the domain interface due to the increase of χ on lowering temperature.

Crystallization of sPP block occurred at 60 s as revealed by the WAXS profiles (see dark cyan curve in Figure 2b). At the same time, a new peak emerged at 0.255 nm^{-1} in the corresponding SAXS profile, and its intensity grew progressively in the expense of the original primary peak at 60 s ≤ t ≤ 300 s. This fact can be seen more clearly by the vertically shifted 1-D SAXS profiles and the time evolution of peak intensity at 0.255 nm^{-1}, as presented in Figures S2a and S2b of the Supporting Information, respectively. A set of scattering

dx.doi.org/10.1021/ma300711k | *Macromolecules* 2012, 45, 5114−5127

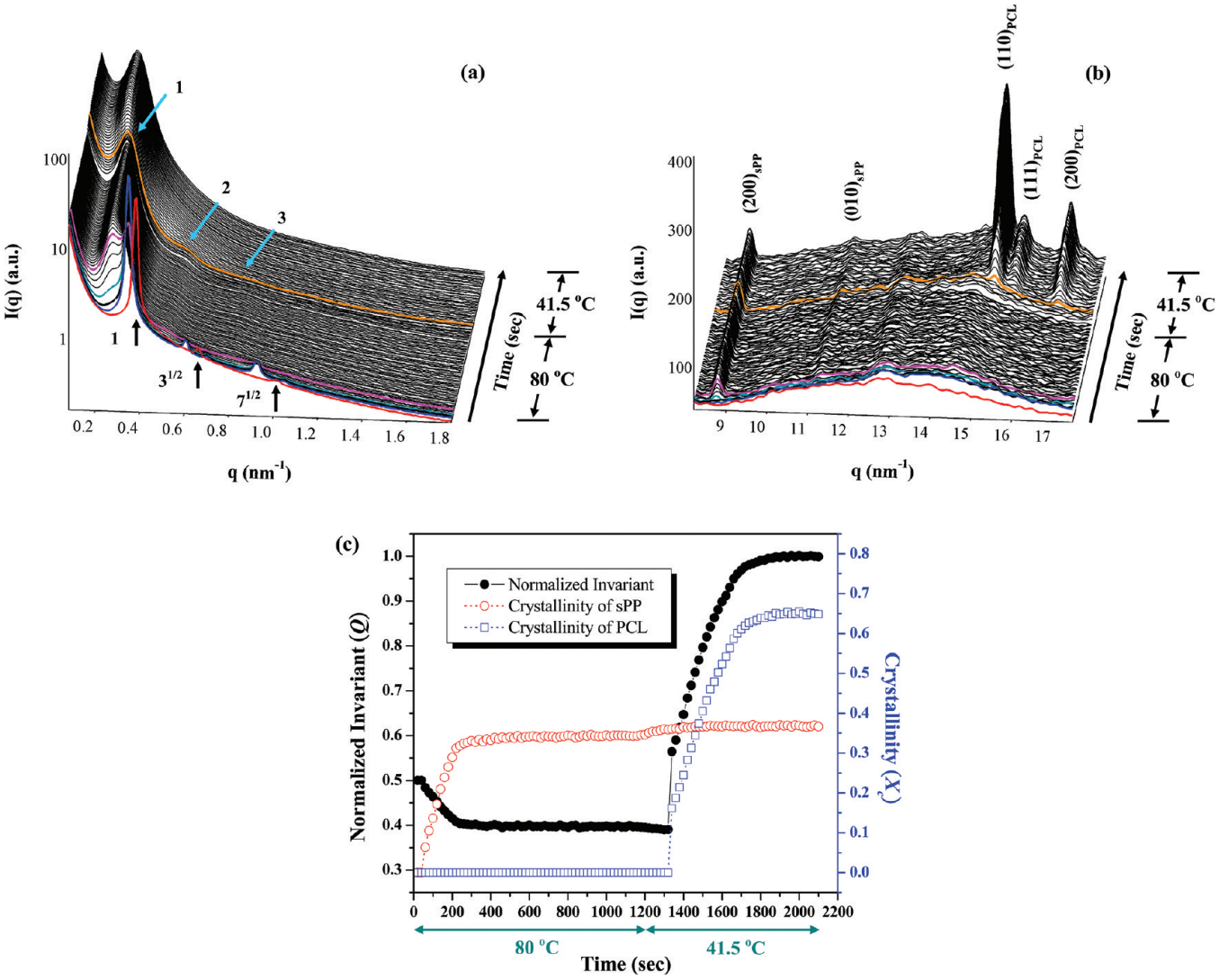

Figure 2. (a) Time-resolved SAXS profiles and (b) time-resolved WAXS profiles of sPP-*b*-PCL subjecting to a two-stage crystallization (the time interval between each profile is 20 s). The system was quenched from 170 to 80 °C to allow sPP crystallization for 20 min followed by quenching to 41.5 °C for PCL crystallization for 15 min. The profiles presented in red, blue, dark cyan, and orange color are associated with the melt mesophase at 170 °C, equilibration at 80 °C for 20 s, the onset of sPP crystallization, and the onset of PCL crystallization, respectively. (c) The normalized invariant (Q) and the crystallinities (X_c) of sPP and PCL blocks as a function of time in the two-stage crystallization process.

peaks with integral position started to appear at 140 s, signaling the morphological transformation from hexagonally packed cylinder to lamellae induced by sPP crystallization. The crystallinity of sPP was found to reach the saturated value of 36% after 300 s.

When the system was subsequently quenched to 41.5 °C, the crystallization of PCL blocks occurred at 140 s, as evidenced by the WAXS profiles (cf. the orange curve in Figure 2b). During the PCL crystallization, the primary peak of the corresponding SAXS profile became broader and the higher-order peaks diminished, revealing that the crystallization of PCL blocks distorted the order of lamellar stacking. The position of the primary peak only showed slight shift toward lower q (comparing the red and blue curves in Figure 1), showing that the lamellar morphology prescribed by sPP crystallization was essentially unperturbed upon PCL crystallization. This indicated that the crystallization of PCL block proceeded within the confined space established by the prior crystallization of the sPP component.

To gain deeper insight into the mechanism of the crystallization, the normalized invariant (Q) and the crystallinities (X_c) obtained from SAXS and WAXS profiles, respectively, are shown in Figure 2c as a function of time. When the diblock was quenched from 170 to 80 °C, sPP blocks started to crystallize at 60 s, and the crystallinity grew progressively in the range of 60 s $\leq t \leq$ 300 s. Meanwhile, the corresponding invariant was found to decrease significantly with increasing sPP crystallinity, primarily due to the reduction of the electron density contrast between sPP and PCL phase upon sPP crystallization (the electron density of crystalline sPP = 326.8 e/nm^3; amorphous sPP = 292.4 e/nm^3; crystalline PCL = 392.9 e/nm^3; amorphous PCL = 350.3 e/nm^3).[52−54] The crystallinity of sPP remained almost saturated after 300 s, and the corresponding invariant did not change apparently. When the system was subsequently quenched to 41.5 °C, PCL block was found to start crystallizing at 140 s after reaching the temperature and finished its crystallization after 720 s. The onset of PCL crystallization was concomitantly accompanied by

dx.doi.org/10.1021/ma300711k | *Macromolecules* 2012, 45, 5114−5127

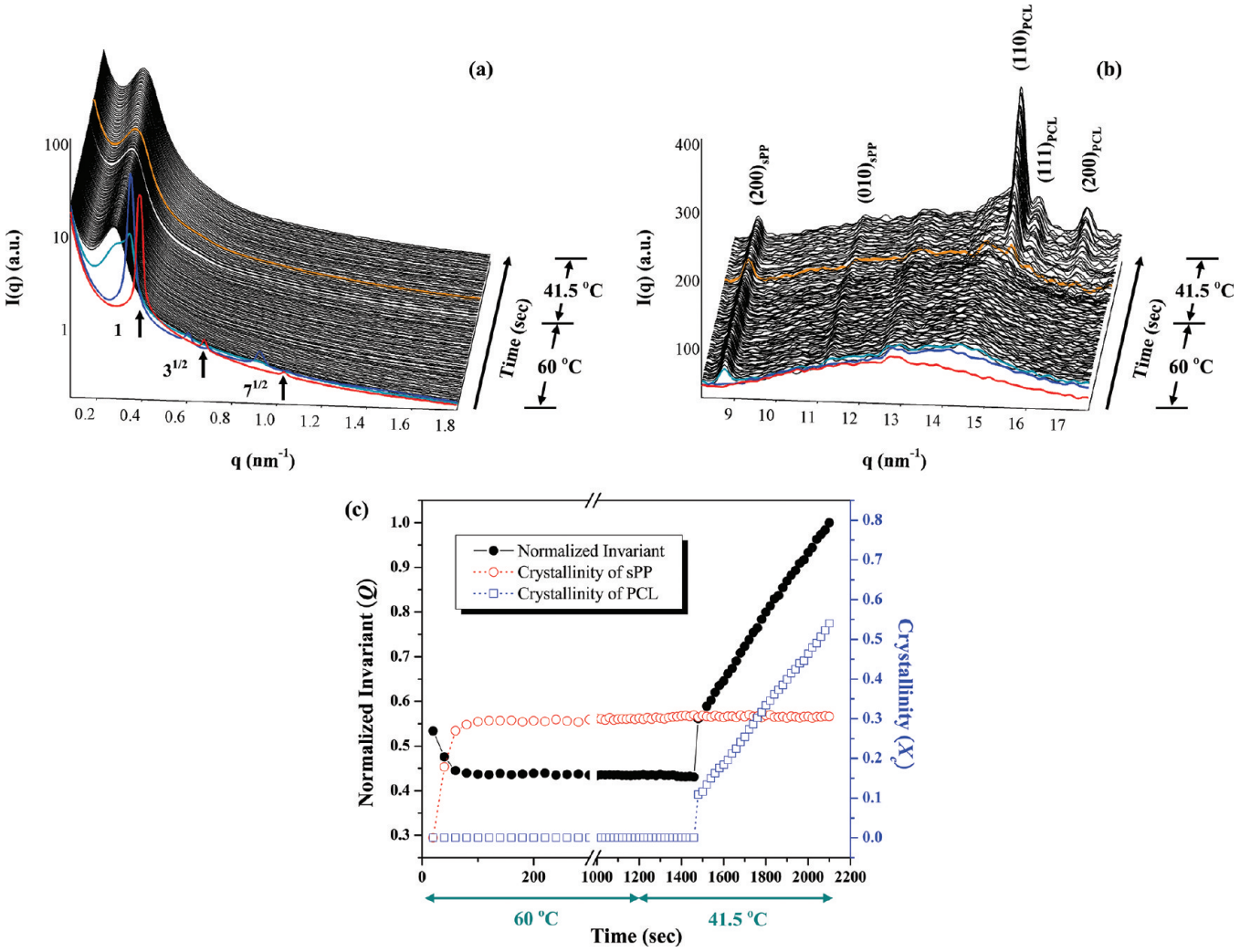

Figure 3. (a) Time-resolved SAXS profiles and (b) time-resolved WAXS profiles of sPP-*b*-PCL subjecting to a two-stage crystallization (the time interval between each profile is 20 s). The system was quenched from 170 to 60 °C to allow sPP crystallization for 20 min followed by quenching to 41.5 °C for PCL crystallization for 15 min. The profiles presented in red, blue, dark cyan, and orange color are associated with the melt mesophase at 170 °C, equilibration at 60 °C for 20 s, the onset of sPP crystallization, and the onset of PCL crystallization, respectively. (c) The normalized invariant (Q) and the crystallinities (X_c) of sPP and PCL blocks as a function of time in the two-stage crystallization process.

an abrupt increase of invariant, which was attributable to the enhancement of the electron density contrast.

Figures 3a and 3b show the time-resolved SAXS/WAXS results of sPP-*b*-PCL, subjecting to a two-stage crystallization with larger undercooling for the first stage, where the sample was quenched from 170 to 60 °C to allow sPP crystallization, followed by quenching to 41.5 °C for PCL crystallization. It can be seen from Figure 3b that upon reaching 60 °C, the crystallization of sPP block took place immediately at 40 s (cf. dark cyan curve), and the crystallinity reached saturation after 120 s. At 40 s $\leq t \leq$ 60 s, the new SAXS peak at 0.27 nm^{-1} grew in expense of the original SAXS peak associated with the melt morphology, indicating again that the sPP crystallization disrupted the melt structure and transformed it into a lamellar morphology. Such a process completed within just 60 s. It is noted that the higher-order peaks associated with the crystalline lamellar morphology were not clearly observed in the SAXS profiles, implying the poorer coherent order of the lamellar stacking due to very rapid sPP crystallization at the larger undercooling. As the system was further quenched to 41.5 °C to induce PCL crystallization, the position of the primary peak did not change obviously, illustrating again that the crystallization of PCL block did not perturb the lamellar morphology further.

Figure 3c shows the corresponding normalized invariant and sPP and PCL crystallinities. The dependence of the invariant on the crystallization time was in accord with the variation of the crystallinities of sPP and PCL blocks, where a decrease and an increase of the invariant during sPP and PCL crystallization, respectively, was mainly associated with the alteration of electron density contrast between these two constituting domains. sPP block was found to crystallize within 40 s upon reaching at 60 °C, and its crystallinity reached saturation after only 120 s. Interestingly, the crystallization rate of PCL block was found to be slower than that observed in the first crystallization history (where T_c^{sPP} = 80 °C) although T_c^{PCL} was identical (i.e., 41.5 °C). It can be seen that for the present crystallization history (where T_c^{sPP} = 60 °C) PCL block started to crystallize at 280 s when the temperature was equilibrated at 41.5 °C, and the crystallinity increased slowly without approaching saturation in 15 min. This result demonstrated that the crystallization kinetics of PCL blocks behaved

dx.doi.org/10.1021/ma300711k | *Macromolecules* 2012, 45, 5114–5127

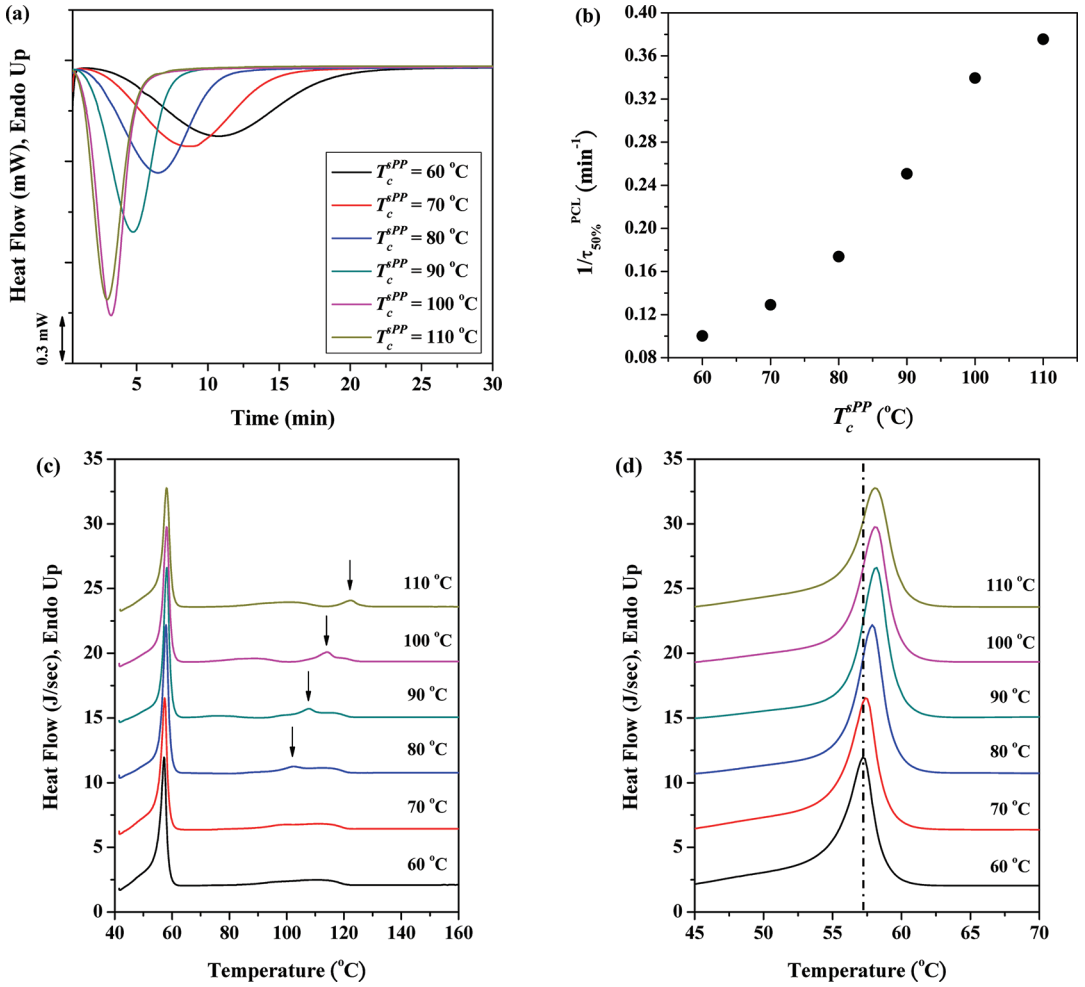

Figure 4. (a) DSC isothermal crystallization scans for the PCL block at 41.5 °C. The measurements were performed after the sPP block was precrystallized at the indicated T_c^{sPP} until saturation. (b) Inverse of the crystallization half-time ($1/\tau_{50\%}$) as a function of T_c^{sPP} obtained from the Avrami analysis for PCL block crystallized at 41.5 °C. (c) DSC heating scans after sPP and PCL block have crystallized at the indicated T_c^{sPP} and 41.5 °C, respectively. (d) Enlarged thermogram around the melting region of PCL block.

differently when the neighboring sPP block was precrystallized at different temperatures (i.e., 60 °C vs 80 °C; see Figures 3c and 2c, respectively).

To confirm that the crystallization kinetics of PCL block was strongly affected by T_c^{sPP} of the prior crystallization of sPP block, the isothermal crystallization of PCL block was systematically studied by DSC. We first allowed the sPP block to crystallize at a prescribed temperature (i.e., T_c^{sPP} = 60−110 °C) until saturation, and then the temperature was lowered rapidly (at 80 °C/min) to 41.5 °C to induce PCL crystallization. The exotherms observed during PCL crystallization are displayed in Figure 4a. It can be seen that when the sPP block was precrystallized at the higher temperature, the crystallization rate of the PCL block at 41.5 °C was faster. For instance, the crystallinity of PCL block was found to reach almost saturation after 12.5 min, but it still kept growing after 15 min when sPP block was precrystallized at T_c^{sPP} = 80 and 60 °C, respectively. This observation is consistent with the time-revolved SAXS/WAXS results presented in Figures 2c and 3c. The data obtained from Figure 4a were further quantitatively analyzed by the Avrami equation.[50] The overall crystallization rate, expressed as the inverse of the crystallization half-time ($1/\tau_{50\%}$), of the PCL block is shown in Figure 4b as a function of T_c^{sPP}. The overall crystallization kinetics of PCL block was seen to increase clearly with increasing T_c^{sPP}.

The subsequent DSC heating scans of sPP-*b*-PCL after sPP and PCL block have crystallized at T_c^{sPP} and 41.5 °C, respectively, are displayed in Figure 4c. The heating trace shows a sharp peak (at ca. 57.5 °C) along with a small endotherm (at 80−125 °C) associated with the melting of PCL and sPP crystals, respectively. The sPP melting peak gradually shifted toward higher temperature with increasing T_c^{sPP}, indicating that the crystallization at higher T_c^{sPP} produced thicker sPP crystals. It is quite interesting to note that different crystal thickness prescribed by sPP crystallization also influenced the melting behavior of the neighboring PCL blocks. The melting region of PCL crystals displayed in Figure 4d revealed that PCL melting point increased with increasing T_c^{sPP}, but it leveled off at $T_c^{sPP} \geq 100$ °C. This observation may be attributed to the greater stretching the PCL block chains (to be demonstrated later by the SAXS results) when the neighboring sPP block was precrystallized at higher T_c^{sPP}. The lower conformational entropy of the more stretched PCL chains reduced the entropy of melting and hence increased T_m^{PCL}.

The nucleation and crystal growth kinetics of the PCL block influenced by sPP crystallization can also be investigated by

dx.doi.org/10.1021/ma300711k | *Macromolecules* 2012, 45, 5114−5127

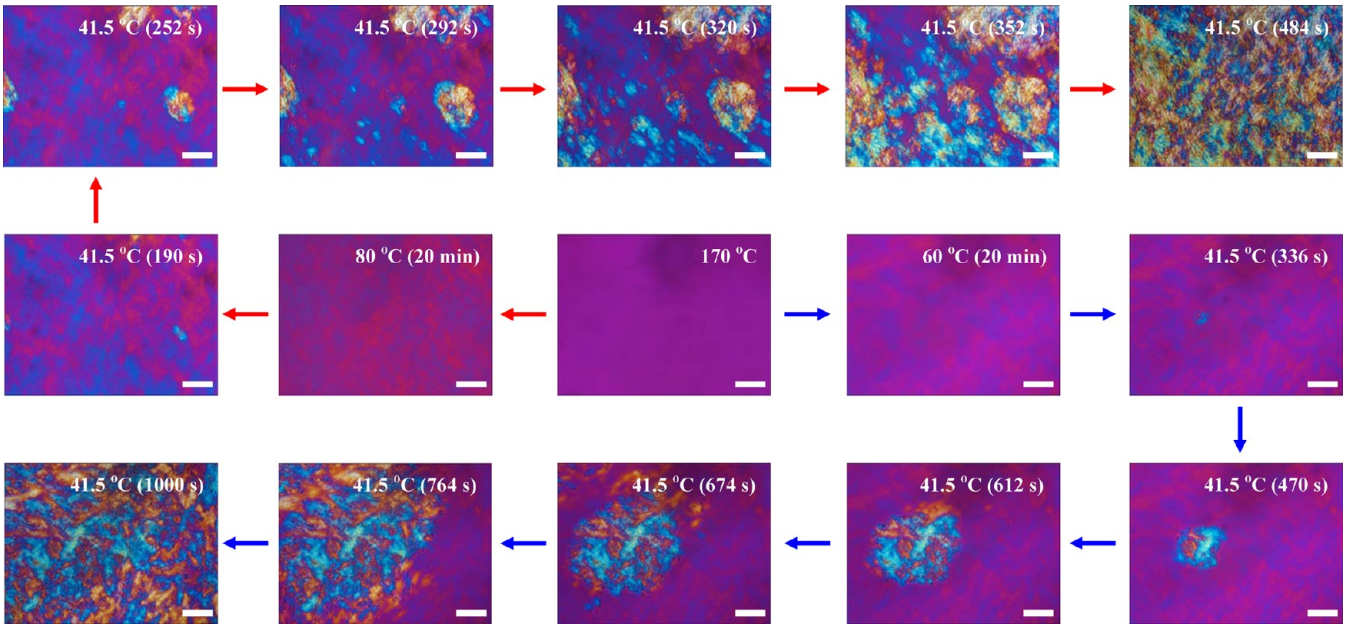

Figure 5. Polarized optical micrographs of sPP-*b*-PCL subjected to the indicated two-stage crystallization history. The middle micrograph corresponds to the initial melt state at 170 °C. The micrographs starting from the middle to the left and then follow the red arrows correspond to the same crystallization history as that employed for Figure 2 (i.e., 170 °C → 80 °C (for sPP crystallization) → 41.5 °C (for PCL crystallization)). The micrographs starting from the middle to the right and then follow the blue arrows correspond to the same crystallization history as that employed for Figure 3 (i.e., 170 °C → 60 °C (for sPP crystallization) → 41.5 °C (for PCL crystallization)). The scale bar represents 50 μm.

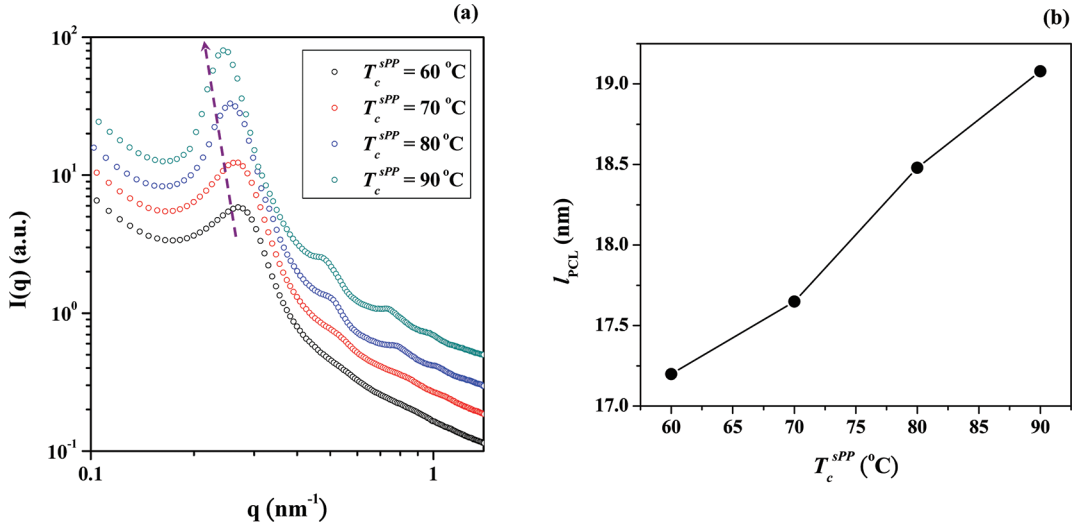

Figure 6. (a) SAXS profiles of sPP-*b*-PCL collected at the indicated T_c^{sPP} (where PCL blocks remained molten state). The sPP block was allowed to crystallize at T_c^{sPP} until saturation before data collection. (b) Variation of the thickness of PCL lamellar microdomain (l_{PCL}) with T_c^{sPP} obtained from the SAXS profiles in (a).

POM. Figure 5 shows the POM micrographs of the sPP-*b*-PCL subjected to the two-stage crystallization histories with T_c^{sPP} = 80 and 60 °C. At 170 °C, no discernible birefringence pattern was observed, indicating that the sPP-*b*-PCL was in the melt state. When the diblock was cooled from 170 to 80 °C and equilibrated there for 20 min, the birefringence texture arising from the crystallization of sPP blocks was identified. When the temperature was subsequently cooled to 41.5 °C, a small number of granular objects with stronger birefringence formed due to the crystallization of PCL block. As the crystallization proceeded further, a bust of many other nuclei occurred followed by prompt growth (with the growth rate of G = 18.0 μm/min), such that the region under observation was quickly filled by PCL crystals within 484 s. However, when the sPP block was precrystallized at 60 °C for 20 min (the sPP birefringence pattern was similar to that found at 80 °C), the kinetics of the subsequent PCL crystallization became quite different. It can be seen that the occurrence of the crystalline texture of PCL was deferred to 336 s; moreover, both the nucleation density and the growth rate (G = 15.4 μm/min) were found to significantly retard as compared to the case for T_c^{sPP} = 80 °C. This fact strongly illustrated that the crystallization of the leading component (i.e., sPP block) affected both the nucleation rate and the crystal growth kinetics for the subsequent crystallization of the other block. The prior crystallization of sPP block at higher T_c^{sPP} was found to

dx.doi.org/10.1021/ma300711k | *Macromolecules* 2012, 45, 5114–5127

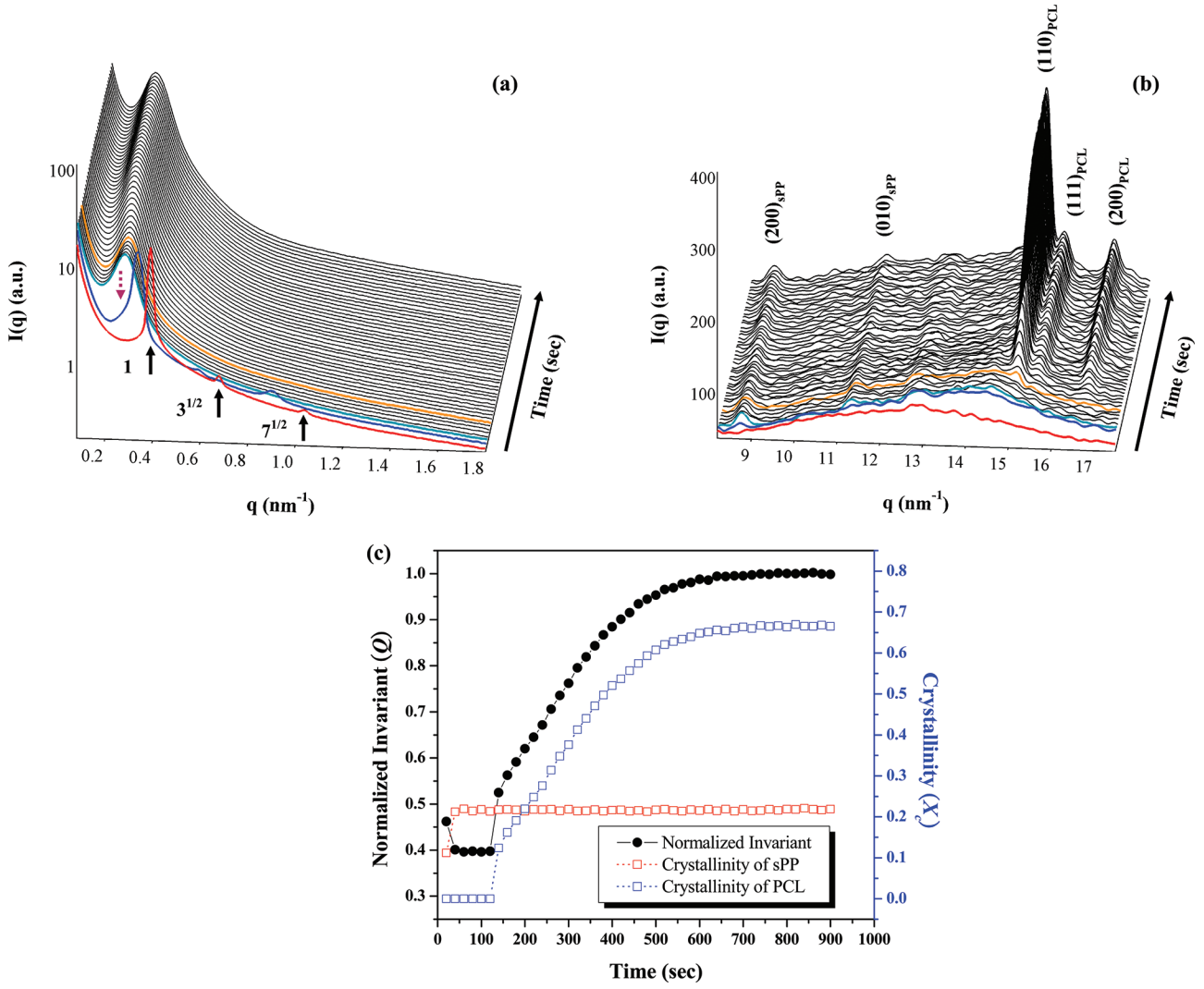

Figure 7. (a) Time-resolved SAXS profiles and (b) time-resolved WAXS profiles of sPP-*b*-PCL subjecting to a one-stage crystallization (the time interval between each profile is 20 s). The system was quenched from 170 to 41.5 °C to allow the crystallizations of both sPP and PCL blocks for 15 min. The profiles presented in red, blue, and orange color are associated with the melt mesophase at 170 °C, the onset of sPP crystallization, and the onset of PCL crystallization, respectively. (c) Normalized invariant (Q) and the crystallinities (X_c) of sPP and PCL blocks as a function of time in the one-stage crystallization process.

promote the nucleation rate more pronouncedly than the growth rate of the PCL crystallization.

Our time-resolved SAXS/WAXS, DSC, and POM results have thus demonstrated that the crystallization rate of PCL block was strongly influenced by the crystallization temperature of the leading crystalline component (i.e., sPP) in the two-stage crystallization process. This type of "interactive crystallization kinetics" has also been observed for a symmetric PLLA-*b*-PEO.[34] In contrast to the present sPP-*b*-PCL, this system was in the disordered state above the melting points of both blocks. When the diblock was brought to T_c^{PLLA} ($T_m^{PEO} < T_c^{PLLA} < T_m^{PLLA}$), a crystalline lamellar morphology was formed by the PLLA crystallization. The thickness of PEO lamellar domain increased with increasing T_c^{PLLA}, implying that the thicker PLLA crystals formed at higher T_c^{PLLA} reduced the cross-sectional area of the junction points at the microdomain interface so as to cause greater stretching of the PEO blocks. The more stretched chain conformation before crystallization enhanced the primary nucleation rate of PEO upon cooling to $T_c^{PEO} < T_m^{PEO}$;[34] therefore, faster PEO crystallization was observed when the PLLA block was allowed to crystallize at higher T_c^{PLLA}. The effect of the crystal thickness (prescribed by the first-crystallized component) on the kinetics of the subsequent crystallization of the lower melting block has also been reported in a recent simulation study by Li et al.[55]

To examine if the degree of stretching of PCL block was influenced by T_c^{sPP}, the SAXS profiles after the crystallization of sPP block were collected at various T_c^{sPP}. It can be seen in Figure 6a that the primary scattering peak shifted progressively to lower q with increasing T_c^{sPP}, indicating swelling of the interlamellar distance (L). The thickness of PCL layers (l_{PCL}) calculated by $l_{PCL} = f_{PCL}L$ (where f_{PCL} is the volume fraction of PCL block) was further found to increase with increasing T_c^{sPP} (Figure 6b), indicating that the PCL blocks did become more stretched after sPP crystallization at higher T_c^{sPP}. Since the chain stems in the sPP crystals aligned normal to the lamellar interface (see Figure S3 and its relevant information in the Supporting Information), the formation of thicker sPP crystals at higher T_c^{sPP} would swell the lamellar domains and hence reduced the cross-sectional areas of the junction points, which

dx.doi.org/10.1021/ma300711k | *Macromolecules* 2012, 45, 5114−5127

then caused the PCL blocks to undergo a stronger stretching normal to the interface. Consequently, the interactive crystallization behavior exhibited by the present sPP-*b*-PCL system may have the same origin as that associated with the PLLA-*b*-PEO system. However, the interactive crystallization kinetics observed in the present sPP-*b*-PCL was distinguished from that of PLLA-*b*-PEO in that the crystallization of the leading crystalline component (i.e., PLLA) in PLLA-*b*-PEO occurred from the disordered melt, whereas sPP in sPP-*b*-PCL crystallized from the microphase-separated melt. Moreover, our results showed that even though the composition of the leading crystalline component (i.e., sPP) was minor, its crystallization (which led to a moderate level of crystallinity) was sufficient to influence the stretching of the majority lower melting block (i.e., PCL block), so as to affect its crystallization kinetics.

In addition to the mediation of PCL chain stretching by sPP crystallization, we would also like to point out (and then preclude) other possible factors that may cause the interactive crystallization behavior in C−C diblock. After the sPP crystallization, the amorphous PCL blocks were attached to the sPP crystallites; these hard "bricks" may lower the mobility of the PCL blocks comparing to the case where they were connected to amorphous sPP. It may hence be argued that the crystallization of PCL block would be slowed down more if the crystallinity of sPP block is higher. Figure S4 shows the crystallinity of sPP block as a function of T_c^{sPP} calculated from the enthalpy of melting. The sPP crystallinity was found to remain nearly constant with respect to the change of T_c^{sPP}; consequently, the possibility arising from effect of crystallinity was precluded.

In Figure 6a, it was observed that the SAXS profile displayed sharper primary peak along with clear higher-order peaks at higher T_c^{sPP} (T_c^{sPP} > 70 °C), whereas the primary peak became broader and the higher-order peaks diminished at lower T_c^{sPP}. This fact suggested that the grain size of the lamellar domains formed after the breakout crystallization of sPP at higher T_c^{sPP} was larger. It may thus be argued that the larger grain size facilitated the crystal growth of PCL to advance over a longer range, such that the PCL crystallization became faster because of lower required nucleation density. If this was the main factor responsible for the interactive crystallization kinetics, then the PCL crystallization should have exhibited a lower nucleation density when its neighboring sPP block was precrystallized at higher T_c^{sPP} due to larger grain size. However, our POM observation in Figure 5 showed that the PCL nucleation density was actually higher for higher T_c^{sPP}, and it was mainly the enhancement of nucleation rate that caused the faster overall crystallization kinetics. Consequently, we also precluded the factor associated with the grain size effect and concluded that the degree of stretching of PCL blocks influenced by sPP crystallization was responsible for the observed interactive crystallization behavior.

3. Crystallization Behavior in the One-Stage Crystallization Process. We now turn our attention to the other type of crystallization history, namely, one-stage crystallization. Figure 7a,b shows the time-resolved SAXS/WAXS profiles of sPP-*b*-PCL, subjected to the one-stage crystallization by direct quenching the diblock from 170 to 41.5 °C. Upon cooling to 41.5 °C for 20 s, the primary peak in the SAXS profile shifted slightly to lower q (see the blue curve in Figure 7a), corresponding to an expansion of the interdomain distance between cylindrical microdomains of 20.9 nm due to the increase of χ. Meanwhile, a low degree of sPP crystallinity was observed in the corresponding WAXS profile (cf. the blue curve in Figure 7b). Such a low crystallinity gave rise to a vague peak hidden at 0.277 nm^{-1} in the corresponding SAXS profile (as indicated by an arrow over the blue curve) under the primary peak due to the breakout crystallization. After 40 s where the crystallinity of sPP nearly reached saturation, the SAXS profile was dominated by the peak at 0.277 nm^{-1}. The perturbation of the SAXS pattern was almost identical to that observed at 60 °C for the sample subjecting to the two-stage crystallization (but the associated structural transformation was faster than that occurred at 60 °C), confirming that a breakout of melt structure driven by sPP crystallization took place to form the crystalline lamellar morphology. The PCL block was found to start crystallizing at 140 s, and the crystallization process was completed after 700 s. Upon PCL crystallization, the primary SAXS peak shifted slightly to lower q, revealing that the crystallization of PCL blocks was essentially confined within the confined space established after the sPP crystallization. The correlation between the scattering invariant and the crystallinities of sPP and PCL blocks as a function of time can be seen in Figure 7c. The time variation of the invariant again agreed well with the change of electron density contrast between sPP and PCL domain during their respective crystallization, as has been discussed earlier.

For the one-stage cooling to 41.5 °C, the WAXS result indicated that sPP actually crystallized before PCL block. Therefore, the crystallization was effectively a two-stage process with T_c^{sPP} = 41.5 °C; however, the PCL crystallization (which was shown to be influenced by the prior crystallization of sPP blocks) now appeared to be faster than that in the two-stage process with T_c^{sPP} = 60 °C (this fact was further confirmed by the isothermal crystallization experiment of DSC, as shown in Figure S5). If the degree of PCL chain stretching dominated the crystallization kinetics, the crystallization rate of PCL block should have been slower for T_c^{sPP} = 41.5 °C compared to the case of T_c^{sPP} = 60 °C. The discrepancy may be explained by considering the stronger hindrance to the breakout of melt structure induced by sPP crystallization at the relatively low T_cs adopted in the one-stage crystallization. Although the SAXS profile indicated a significant morphological breakout upon sPP crystallization at 41.5 °C, the degree of structural perturbation should not be the same as that attained in the two-stage process considering that the saturated crystallinity of sPP at 41.5 °C was obviously lower (0.22 compared to the value of 0.31 attained at T_c^{sPP} = 60 °C). It is proposed that at $T_c^{sPP} \leq$ 41.5 °C a significant portion of sPP blocks remained confined within the highly discrete microdomains (e.g., the original cylindrical microdomains or the domains established by local or short-range coalescence of the cylinders), such that they were uncrystallizable at the prescribed T_c^{sPP} because the undercooling was not large enough to induce the homogeneous nucleation. The PCL blocks attached to these discrete domains thus still formed the continuous matrix phase and hence crystallized more rapidly than the case when they were confined within the lamellar domains generated by the breakout crystallization of sPP at higher T_c^{sPP}. Moreover, since the sPP crystallinity attained at 41.5 °C was significantly smaller than that developed at higher T_c^{sPP}, there were less PCL blocks attached to the sPP crystallites (which would reduce the mobility of PCL blocks). This may also contribute to the faster PCL crystallization comparing to that at T_c^{sPP} = 60 °C.

The crystallization temperature of 41.5 °C in the one-stage process still allowed the sPP crystallization to take place before

dx.doi.org/10.1021/ma300711k | *Macromolecules* 2012, 45, 5114−5127

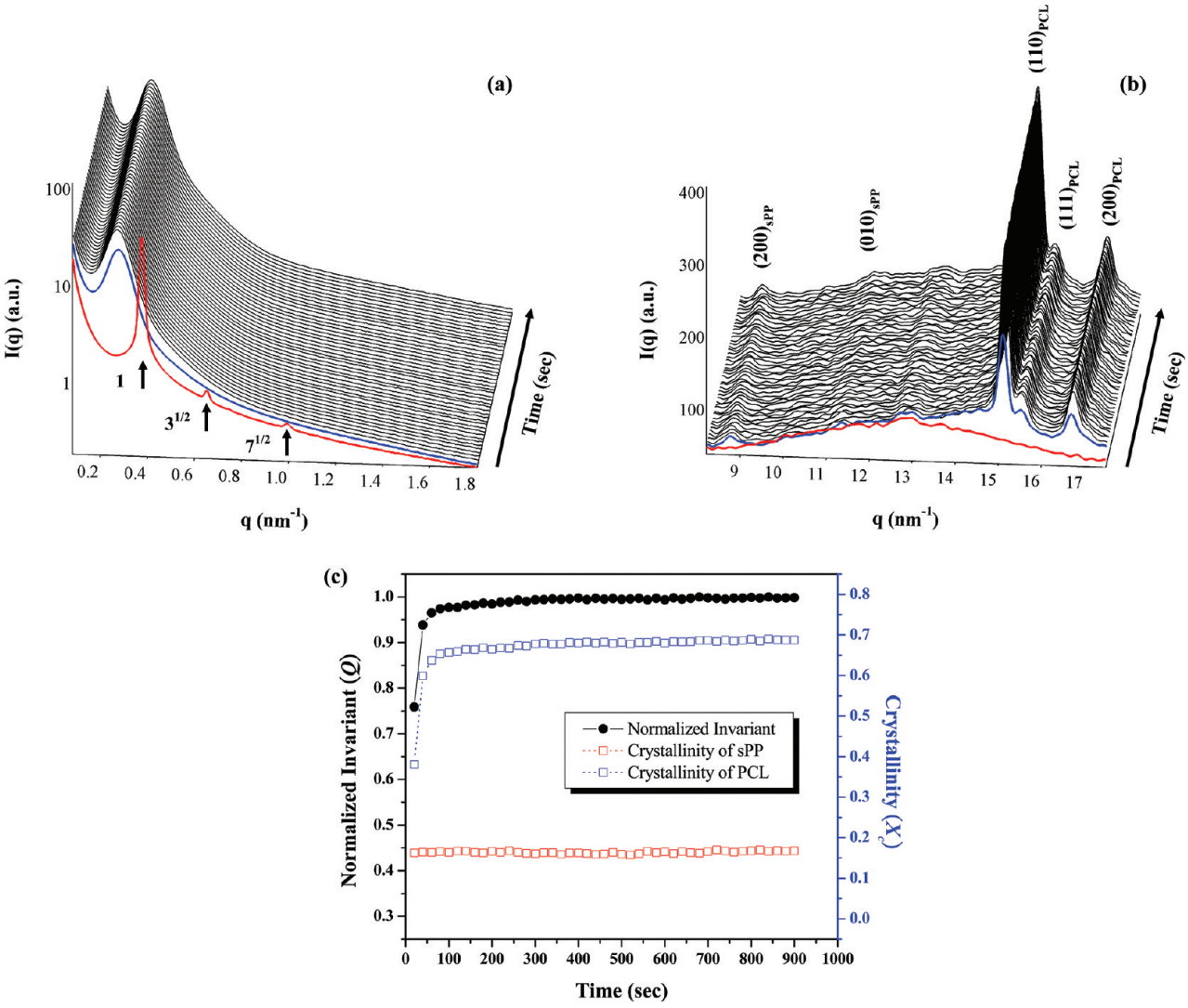

Figure 8. (a) Time-resolved SAXS profiles and (b) time-resolved WAXS profiles of sPP-*b*-PCL subjecting to a one-stage crystallization (the time interval between each profile is 20 s). The system was quenched from 170 to 30 °C to allow the crystallizations of both sPP and PCL blocks for 15 min. The profiles presented in red and blue color are associated with the melt mesophase at 170 °C and the onset of the concurrent crystallization of sPP and PCL blocks, respectively. (c) Normalized invariant (Q) and the crystallinities (X_c) of sPP and PCL blocks as a function of time in the one-stage crystallization process.

the crystallization of PCL block. It would be of interest to examine if the competitiveness of the two crystallization events may be enhanced by further lowering the crystallization temperature. Figure 8a,b displays the time-resolved SAXS/WAXS profiles of sPP-*b*-PCL collected upon quenching from 170 to 30 °C. At 20 s, the crystallizations of both sPP and PCL blocks started to take place almost simultaneously, as evidenced by the WAXS profile (see the blue curve in Figure 8b). At the same time, the corresponding SAXS profile showed a broad peak, signaling that the initial melt morphology was disrupted by the concurrent crystallization of sPP and PCL blocks. The crystallinities of both blocks approached nearly constant after 60 s. The time evolutions of invariant and crystallinities of sPP and PCL blocks are shown in Figure 8c. Since two crystallization events occurred almost simultaneously and the crystallinities reached saturation rapidly, the corresponding invariant was governed by the electron density contrast between crystalline sPP and crystalline PCL domains. The ultimate sPP crystallinity attained here was significantly suppressed to 0.17 (cf. Figure 8c), indicating that the long-range breakout of the sPP mcirodomains induced by crystallization at 30 °C was even more difficult.

Figure 9a,b shows the time-resolved SAXS/WAXS profiles of sPP-*b*-PCL collected by direct quenching the diblock from 170 to 10 °C. PCL block was found to start crystallizing when the temperature was just brought to 10 °C, and its crystallinity promptly reached saturation after 60 s. However, the crystallization of sPP block did not take place within the maximum data collection time (i.e., 15 min), as the crystalline diffraction peaks of sPP were absent in the WAXS profiles (cf. Figure 9b). Upon reaching 10 °C, the primary SAXS peak shifted slightly to lower q as compared to that in the melt state, and two higher-order peaks with the position ratio of $3^{1/2}$ and $7^{1/2}$ were still observable (see the blue curve in Figure 9a), indicating that the hexagonally packed cylinder morphology was still preserved. The shift of the primary peak corresponded to an increase of D by 3.1 nm, which was attributed to the increasing stretching of the amorphous sPP and PCL blocks due to the increase of χ by lowering the temperature to 10 °C . Figure 9c shows the dependences of invariant and crystallinities

dx.doi.org/10.1021/ma300711k | *Macromolecules* 2012, 45, 5114–5127

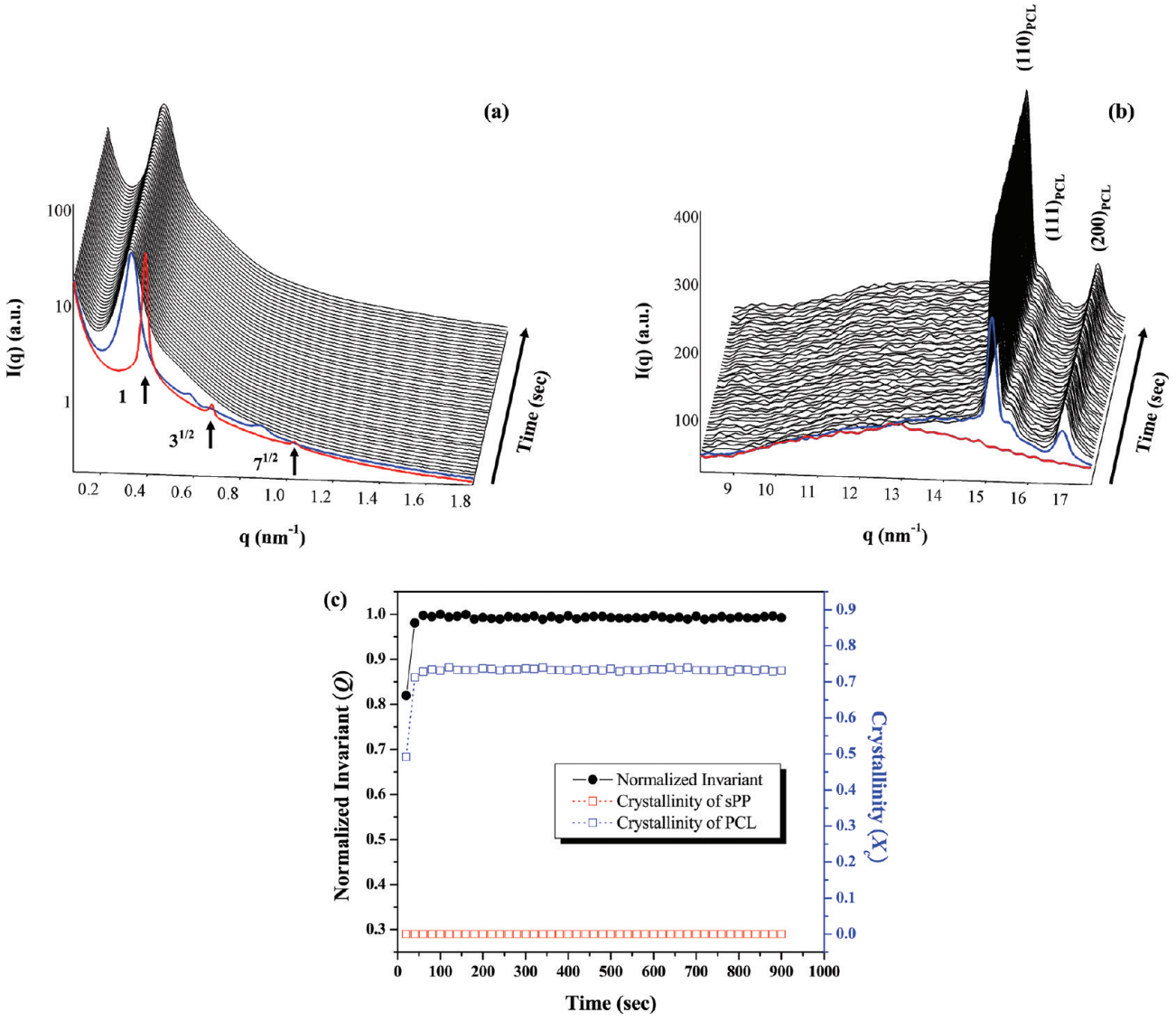

Figure 9. (a) Time-resolved SAXS profiles and (b) time-resolved WAXS profiles of sPP-*b*-PCL subjecting to a one-stage crystallization (the time interval between each profile is 20 s). The system was quenched from 170 to 10 °C to allow the crystallizations of both sPP and PCL blocks for 15 min. The profiles presented in red and blue color are associated with the melt mesophase at 170 °C and the onset of the crystallization of PCL block, respectively. (c) The normalized invariant (Q) and the crystallinities (X_c) of sPP and PCL blocks as a function of time in the one-stage crystallization process.

of sPP and PCL blocks on crystallization time. The PCL crystallization before 60 s led to an abrupt increase of invariant. It is worth noting that the primary SAXS peak slightly broadened without changing the position and the higher-order peaks (with the position ratio of $3^{1/2}$ and $7^{1/2}$) disappeared after 40 s, signaling that the crystallization of PCL block disturbed the long-range order of the sPP cylindrical microdomains while retaining the average interdomain distance. Since the sPP blocks still formed the cylindrical domains embedded in the semicrystalline PCL matrix, the crystallization in the minority of the sPP domains had to proceed through homogeneous nucleation which requires exceedingly large undercooling.[12] But the degree of undercooling prescribed by the crystallization temperature of 10 °C was not sufficiently large to induce such a nucleation process, such that the sPP block remained uncrystallizable at this temperature.

CONCLUSIONS

A double-crystalline sPP-*b*-PCL with an asymmetric composition has been studied by considering two types of crystallization history. In the two-stage crystallization, it was demonstrated that when the sPP block was precrystallized at higher temperature, the kinetics of the subsequent crystallization of PCL blocks was faster. This interactive crystallization behavior was ascribed mainly to the degree of stretching of PCL blocks influenced by sPP crystallization; that is, the formation of thicker sPP crystals at higher T_c^{sPP} induced greater stretching of the PCL blocks, which in turn enhanced the primary nucleation rate associated with the PCL crystallization.

In the one-stage crystallization process, decreasing the crystallization temperature was found to enhance the competitiveness of sPP and PCL crystallization. However, the degree of morphological perturbation induced by the breakout crystallization of sPP block became increasingly difficult with decreasing T_c, such that a significant portion of sPP blocks

dx.doi.org/10.1021/ma300711k | *Macromolecules* 2012, 45, 5114−5127

remained confined within the highly discrete microdomains which were either the original cylindrical domains formed in the melt or the domains established by local coalescence of the sPP cylinders. These sPP blocks remained uncrystallizable at the T_cs studied here because the corresponding undercoolings were not large enough to induce the homogeneous nucleation.

■ ASSOCIATED CONTENT

Supporting Information

Avrami plot for the isothermal crystallization of sPP block in sPP-*b*-PCL; the vertically shifted time-resolved SAXS profiles and the normalized intensity of the new peak emerged at 0.255 nm^{-1} in the SAXS profiles (corresponding to Figure 2a) as a function of crystallization time; the analysis of orientations of sPP and PCL crystals with respect to the interface of lamellar microdomain; the crystallinity of sPP block formed at different T_c^{sPP}; the comparison of DSC isothermal crystallization exotherms for the PCL block at 41.5 °C. This material is available free of charge via the Internet at http://pubs.acs.org.

■ AUTHOR INFORMATION

Corresponding Author

*E-mail: hlchen@che.nthu.edu.tw.

Notes

The authors declare no competing financial interest.

■ ACKNOWLEDGMENTS

We gratefully appreciate Prof. Stephen Z. D. Cheng at The University of Akron for the valuable discussions and assistance in the DSC isothermal crystallization experiment. We acknowledge the support of the National Science Council, Taiwan, under Grant NSC 99-2221-E-007-008 and the Frontier Center of Fundamental and Applied Sciences of Matters of the National Tsing Hua University. We also thank the National Synchrotron Radiation Research Center for supporting the X-ray scattering experiments at beamline BL23A1 and BL17A1.

■ REFERENCES

(1) Bates, F. S.; Fredrickson, G. H. *Annu. Rev. Phys. Chem.* **1990**, *41*, 525−557.
(2) Bates, F. S.; Fredrickson, G. H. *Phys. Today* **1999**, *52*, 32−38.
(3) Bates, F. S. *Science* **1991**, *251*, 898−905.
(4) Fredrickson, G. H.; Bates, F. S. *Annu. Rev. Mater. Sci.* **1996**, *26*, 501−550.
(5) Leibler, L. *Macromolecules* **1980**, *13*, 1602−1617.
(6) Weimann, P. A.; Hajduk, P. A.; Hajduk, D. A.; Chu, C.; Chaffin, K. A.; Brodil, J. C.; Bates, F. S. *J. Polym. Sci., Part B: Polym. Phys.* **1999**, *37*, 2053−2068.
(7) Arnal, M. L.; Balsamo, V.; Lopez-Carrasquero, F.; Contreras, J.; Carrillo, M.; Schmalz, H.; Abetz, V.; Laredo, E.; Müller, A. J. *Macromolecules* **2001**, *34*, 7973−7982.
(8) Zhu, L.; Cheng, S. Z. D.; Calhoun, B. H.; Ge, Q.; Quirk, R. P.; Thomas, E. L.; Hsiao, B. S.; Yeh, F.; Lotz, B. *Polymer* **2001**, *42*, 9121−9131.
(9) Müller, A. J.; Balsamo, V.; Arnal, M. L.; Jakob, T.; Schmalz, H.; Abetz, V. *Macromolecules* **2002**, *35*, 3048−3058.
(10) Sun, Y. S.; Chung, T. M.; Li, Y. J.; Ho, R. M.; Ko, B. T.; Jeng, U. S.; Lotz, B. *Macromolecules* **2006**, *39*, 5782−5788.
(11) Sun, Y. S.; Chung, T. M.; Li, Y. J.; Ho, R. M.; Ko, B. T.; Jeng, U. S. *Macromolecules* **2007**, *40*, 6778−6781.
(12) Chen, H. L.; Hsiao, S. C.; Lin, T. L.; Yamauchi, K.; Hasegawa, H.; Hashimoto, T. *Macromolecules* **2001**, *34*, 671−674.
(13) Chen, H. L.; Wu, J. C.; Lin, T. L.; Lin, J. S. *Macromolecules* **2001**, *34*, 6936−6944.
(14) Loo, Y. L.; Register, R. A.; Ryan, A. J. *Macromolecules* **2002**, *35*, 2365−2374.
(15) Loo, Y. L.; Register, R. A.; Ryan, A. J. *Phys. Rev. Lett.* **2000**, *84*, 4120−4123.
(16) Loo, Y. L.; Register, R. A.; Adamson, D. H. *Macromolecules* **2000**, *33*, 8361−8366.
(17) Loo, Y. L.; Register, R. A.; Ryan, A. J.; Dee, G. T. *Macromolecules* **2001**, *34*, 8968−8977.
(18) Ho, R. M.; Lin, F. H.; Tsai, C. C.; Lin, C. C.; Ko, B. T.; Hsiao, B. S.; Sics, I. *Macromolecules* **2004**, *37*, 5985−5994.
(19) Nojima, S.; Kato, K.; Yamamoto, S.; Ashida, T. *Macromolecules* **1992**, *25*, 2237−2242.
(20) Nojima, S.; Nakano, H.; Ashida, T. *Polymer* **1993**, *34*, 4168−4170.
(21) Nojima, S.; Nakano, H.; Takahashi, Y.; Ashida, T. *Polymer* **1994**, *35*, 3479−3486.
(22) Nojima, S.; Yamamoto, S.; Ashida, T. *Polym. J.* **1995**, *27*, 673−682.
(23) Hsu, J. Y.; Hsieh, I. F.; Nandan, B.; Chiu, F. C.; Chen, J. H.; Jeng, U. S.; Chen, H. L. *Macromolecules* **2007**, *40*, 5014−5022.
(24) Müller, A. J.; Balsamo, V.; Arnal, M. L. In *Lecture Notes in Physics: Progress in Understanding of Polymer Crystallization*; Reiter, G., Strobl, G., Eds.; Springer: Berlin, 2007; Springer Lecture Notes in Physics Vol. *714*, pp 229−259.
(25) Castillo, R. V.; Müller, A. J. *Prog. Polym. Sci.* **2009**, *34*, 516−560.
(26) Kim, K. S.; Chung, S.; Chin, I. J.; Kim, M. N.; Yoon, J. S. *J. Appl. Polym. Sci.* **1999**, *72*, 341−348.
(27) Maglio, G.; Migliozzi, A.; Palumbo, R. *Polymer* **2003**, *44*, 369−375.
(28) Sun, L.; Liu, Y.; Zhu, L.; Hsiao, B. S.; Avila-Orta, C. A. *Polymer* **2004**, *45*, 8181−8193.
(29) Nojima, S.; Akutsu, Y.; Washino, A.; Tanimoto, S. *Polymer* **2004**, *45*, 7317−7324.
(30) Nojima, S.; Akutsu, Y.; Akaba, M.; Tanimoto, S. *Polymer* **2005**, *46*, 4060−4067.
(31) Hamley, I. W.; Castelletto, V.; Castillo, R. V.; Müller, A. J.; Martin, C. M.; Pollet, E.; Dubois, P. *Macromolecules* **2005**, *38*, 463−472.
(32) Castillo, R. V.; Arnal, M. L.; Müller, A. J.; Hamley, I. W.; Castelletto, V.; Schmalz, H.; Abetz, V. *Macromolecules* **2008**, *41*, 879−889.
(33) Cao, W. Y.; Tashiro, K.; Hanesaka, M.; Takeda, S.; Masunaga, H.; Sasaki, S.; Takata, M. *J. Phys. Chem. B* **2009**, *113*, 2338−2346.
(34) Cong, Y. H.; Liu, H.; Wang, D. L.; Zhao, B. J.; Yan, T. Z.; Li, L. B.; Chen, W.; Zhong, Z. Y.; Lin, M. C.; Chen, H. L.; Yang, C. L. *Macromolecules* **2011**, *44*, 5878−5882.
(35) Nojima, S.; Ono, M.; Ashida, T. *Polym. J.* **1992**, *24*, 1271−1280.
(36) Gan, Z. H.; Jiang, B. Z.; Zhang, J. *J. Appl. Polym. Sci.* **1996**, *59*, 961−967.
(37) Bogdanov, B.; Vidts, A.; Schacht, E.; Berghmans, H. *Macromolecules* **1999**, *32*, 726−731.
(38) Shiomi, T.; Imai, K.; Takenaka, K.; Takeshita, H.; Hayashi, H.; Tezuka, Y. *Polymer* **2001**, *42*, 3233−3239.
(39) Albuerne, J.; Marquez, L.; Müller, A. J.; Raquez, J. M.; Degee, P.; Dubois, P.; Castelletto, V.; Hamley, I. W. *Macromolecules* **2003**, *36*, 1633−1644.
(40) Takeshita, H.; Fukumoto, K.; Ohnishi, T.; Ohkubo, T.; Miya, M.; Takenaka, K.; Shiomi, T. *Polymer* **2006**, *47*, 8210−8218.
(41) Nojima, S.; Fukagawa, Y.; Ikeda, H. *Macromolecules* **2009**, *42*, 9515−9522.
(42) Castillo, R. V.; Müller, A. J.; Lin, M. C.; Chen, H. L.; Jeng, U. S.; Hillmyer, M. A. *Macromolecules* **2008**, *41*, 6154−6164.
(43) Myers, S. B.; Register, R. A. *Macromolecules* **2008**, *41*, 6773−6779.
(44) Tzeng, F. Y.; Lin, M. C.; Wu, J. Y.; Kuo, J. C.; Tsai, J. C.; Hsiao, M. S.; Chen, H. L.; Cheng, S. Z. D. *Macromolecules* **2009**, *42*, 3073−3085.
(45) Jeng, U. S.; Su, C. H.; Su, C. J.; Liao, K. F.; Chuang, W. T.; Lai, Y. H.; Chang, J. W.; Chen, Y. J.; Huang, Y. S.; Lee, M. T.; Yu, K. L.;

Lin, J. M.; Liu, D. G.; Chang, C. F.; Liu, C. Y.; Chang, C. H.; Liang, K. S. *J. Appl. Crystallogr.* **2010**, *43*, 110−121.
(46) Debye, P.; Bueche, A. M. *J. Appl. Phys.* **1949**, *20*, 518−525.
(47) Debye, P.; Anderson, H. R., Jr.; Brumberger, H. *J. Appl. Phys.* **1957**, *28*, 679−683.
(48) Ruland, W. J. *J. Appl. Crystallogr.* **1971**, *4*, 70−73.
(49) Matsen, M. W.; Bates, F. S. *Macromolecules* **1996**, *29*, 1091−1098.
(50) Avrami, M. *J. Chem. Phys.* **1939**, *7*, 1103−1112; **1940**, *8*, 212−224; **1941**, *9*, 177−184.
(51) Lorenzo, A. T.; Arnal, M. L.; Albuerne, J.; Müller, A. J. *Polym. Test.* **2007**, *26*, 222−231.
(52) Chung, T. M.; Ho, R. M.; Kuo, J. C.; Tsai, J. C.; Hsiao, B. S.; Sics, I. *Macromolecules* **2006**, *39*, 2739−2742.
(53) Chatani, Y.; Okita, Y.; Tadokoro, H.; Yamashita, Y. *Polym. J.* **1970**, *1*, 555−562.
(54) Crescenzi, V.; Manzini, G.; Calzolari, G.; Borri, C. *Eur. Polym. J.* **1972**, *8*, 449−463.
(55) Li, Y.; Ma, Y.; Li, J.; Jiang, X. M.; Hu, W. B. *J. Chem. Phys.* **2012**, *136*, 104906.
(56) Lotz, B.; Lovinger, A. J.; Cais, R. E. *Macromolecules* **1988**, *21*, 2375−2382.
(57) Lovinger, A. J.; Lotz, B.; Davis, D. D.; Padden, F. J. *Macromolecules* **1993**, *26*, 3494−3503.
(58) De Rosa, C.; Corradini, P. *Macromolecules* **1993**, *26*, 5711−5718.
(59) Bittiger, H.; Marchessault, R. H.; Niegisch, W. D. *Acta Crystallogr.* **1970**, *B26*, 1923−1927.
(60) Hu, H. L.; Dorset, D. L. *Macromolecules* **1990**, *23*, 4604−4607.